Nonlocal optical response of assemblies of semiconductor spheres

Yasushi Ohfuti and Kikuo Cho
Faculty of Engineering Science, Osaka University, Toyonaka, Osaka 560, Japan
(Received 28 April 1994; revised manuscript received 6 October 1994)

Linear optical response of assemblies of small semiconductor spheres is studied by using a nonlocal theory. A self-consistent treatment of the Schrödinger and Maxwell equations naturally leads to complex radiative corrections to electronic levels. The size and the dimensionality dependence is examined from the response spectra and the matrix elements of the retarded interaction. For one and two dimensional infinite lattices of the spheres, it is shown analytically that the complex radiative corrections obtained by this semiclassical approach agree with those obtained by QED. The size dependence in finite systems is investigated numerically for some geometries. It is shown that the Coulomb interaction causes a strong geometry dependence of response spectra even if the system is much smaller than the wavelength of resonant light. The size-resonant enhancement of induced polarization is also investigated.

I. INTRODUCTION

Recently, there has been a strong current interest in the study of mesoscopic (MS) systems. A common feature of the interest is the appearance of material coherence in observed quantities. Physical properties of MS systems are expected to depend strongly on the size and shape of samples, because of the coherence of electronic wave functions. This aspect has stimulated the studies of MS systems from both fundamental and applicational points of view.

As to the optical properties of MS systems, the fundamental problem is how to include nonlocality in its theoretical framework in a feasible manner, and the main applicational interest is to find out systems with high optical nonlinearity through optimal combination of size, shape, and internal structure. As a measure of the strength of the radiation-matter interaction H', one usually considers oscillator strength, but a spontaneous emission (SE) rate is more appropriate. Though both of them are directly related to the matrix element of the transition dipole moment, the former is a valid concept only in a long wave approximation (LWA), with the information of field amplitude eliminated. The matrix element of H' reflects both the details of material wave functions and the mode structure of the electromagnetic field, thus depending sensitively on the size, shape, and internal structure of MS systems, and the SE rate is largely affected by putting resonant systems into various cavity structures.[1]

A simple argument of the size dependence of the SE rate is based on the LWA of the transition dipole moment of size-quantized excited states. Within the LWA, i.e., when the sample size is much smaller than the light wavelength, the SE rate (or the radiative width) of size-quantized excited levels[2–5] and the third-order nonlinear polarizability $\chi^{(3)}$ (Refs. 6 and 7) are proportional to the sample volume. There is also an experimental report on the size enhancement of radiative decay rate in a semiconductor microcrystallite in a certain range of sample size.[8]

Though this type of size enhancement of the SE rate occurs for small samples satisfying the LWA condition, infinitely large systems also show an enhanced SE rate. A calculation of the SE rate for crystalline arrays of molecules in one- and two-dimensional lattices shows a larger rate than for a single molecule, and the rate depends strongly on the dimensionality of the array.[9] This calculation makes full use of the translational symmetry, and therefore, is limited to the infinite lattices.

Theoretical studies of the size dependence of the SE rate have been limited to either LWA or infinite crystals, and the size region connecting these two limiting cases has been left unexplored. Its study is one of the main objects of the paper. From this study, it will be elucidated how the size enhancement in the LWA regime becomes saturated through the increasing weight of nonlocality, and how the size-dependent nonuniformity of internal electromagnetic field plays an essential role in the optical response. The present study is based on the framework of nonlocal response theory developed previously.[10] Though it is a direct consequence of quantum mechanics and (microscopic) electromagnetic theory, its appearance is somewhat different from standard theory. Therefore, we give its outline and the relationship with other response theories in Appendix A.

Generally, perturbation at a point can induce response at other points through the coherence of the electronic wave functions.[10] In this sense, the susceptibility is nonlocal. Mathematically, the nonlocal form of the susceptibility function is nothing but a result of application of the perturbation theory to the Schrödinger equation. The current density is given as a functional of the vector potential, while the vector potential is obtained as a functional of the current density plus the free field, by solving the Maxwell equations. Another important feature of the susceptibility function is that the current density is written as the sum of the products of the matrix elements of the current density operators at two positions. This separability feature allows us to reduce the problem to a set of linear equations, whose coefficients contain the

retarded interaction among the induced current densities mediated by radiation fields and give rise to the radiative correction (shift and broadening) to the material levels. This interaction may be called radiation reaction. In the following, we will conventionally use the polarization density and the transverse electromagnetic fields instead of the current density and the vector potential, because those are essentially the same physical quantities.

It is not surprising that the SE rate can be obtained without quantization of light. It is known that the SE can be attributed either to the radiation reaction or the vacuum fluctuation or to both according to the ordering of operators.[11,12] Thus, whether one should ascribe SE to radiation reaction or to vacuum fluctuation is just a problem of interpretation. The radiative decay is explainable semiclassically if we consider the radiation reaction correctly, because the equations of motions are the same and the main part of the radiative decay does not contain the Planck's constant. In fact, it has been shown for a two level model in Ref. 10 that the radiative decay can be correctly obtained from this formalism and we will show it again for infinite periodic array systems.[9]

The nonlocality is essential to a unified description of optical responses from microscopic to macroscopic systems. The size and the shape of the induced polarization density determine the character of the retarded interaction. The shape of the polarization strongly depends on the geometry of the system. It will be shown that the radiative correction is different for different geometries even if the system is much smaller than the wavelength of the resonant light. Careful treatment by the nonlocal theory has also shown that $\chi^{(3)}$ grows linearly with the volume when the system size is small and gets saturated as the size becomes larger.[7]

Another importance of the nonlocality has been pointed out as to the radiative shift in finite systems.[13] The $\chi^{(3)}$ in ω representation has poles at the excitation energies E_λ of unperturbed material systems. Since the susceptibilities are defined perturbationally and described in terms of the variables in unperturbed systems, the energies do not contain the radiation-matter interaction. The energy of pump light is chosen so that the systems are resonantly excited in order to get the strong third-order response. The retardation, however, shifts the resonant energies from E_λ to $\tilde{E}_\lambda$. This causes incompatibility of the resonant conditions for the large $\chi^{(3)}$ and for the large induced dipole moment density. When the size (or the shape) of the system is changed, the radiative shift changes as well as E_λ's subject to the boundary condition. It may happen that $E_\lambda = \tilde{E}_\mu$ for $\lambda \neq \mu$. In this case, the two conditions mentioned above can be satisfied simultaneously and we can expect a large nonlinear signal. The spatial form of the induced dipole density is unlike that of the incident field, because the dipole density corresponding to the state μ is dominant. This effect may be called "nonlocality induced double resonance in energy and size (NIDORES)."[14] Although the NIDORES effect is referred to the nonlinear processes, its condition can be fixed within the linear response.

In this paper, we study the linear optical response of various assemblies of small semiconductor spheres, using the nonlocal theory. Changing the number and the arrangement of the spheres, we examine the size and the dimensionality dependence from the response spectra or more directly from the matrix elements of the retarded interaction. The matrix elements can be evaluated analytically for a single sphere and infinite lattices of the spheres. Comparison with the results obtained for molecular systems by QED (Ref. 9) shows that the same complex radiative shift can be obtained also from the semiclassical approach. A sum rule is derived for the radiative widths. It is shown that the sum of the radiative widths of all the modes is the sum of those of individual spheres. The main part of the radiative widths is, however, concentrated on the modes whose averaged wave numbers are smaller than the wave number of the resonant light. The radiative width is monopolized by the mode with the largest dipole moment, when the system size is smaller than the wavelength of the resonant light. The responses of finite systems are investigated numerically. The size dependence is simple for a linear system. The behavior can be understood from the analytic consideration. In two and three dimensional systems, the behavior is more complicated, due to the long range nature of the dipole-dipole interaction. The NIDORES condition is also investigated.

In Sec. II, we summarize the nonlocal formulation which is to be used. The model is introduced in Sec. III. In Sec. IV, we analyze the matrix elements of the retarded interaction. Comparison with the results of a QED calculation is made for a single sphere and periodic systems. Section V gives numerical results for finite systems. Section VI is devoted to a discussion and concluding remarks.

II. FORMULATION

We here just summarize the part of the formulation that we are to use. The detail is described in Ref. 10. The essential point is the self-consistent determination of induced polarization and corresponding electromagnetic field (or the current density and the vector potential) by solving Maxwell and Schrödinger equations simultaneously. Solving the Schrödinger equation with the vector potential $\mathbf{A}$ (in Coulomb gauge, i.e., $\mathrm{div}\mathbf{A} = 0$) perturbationally to the first order, we have the polarization given as

$$\mathbf{P}(\mathbf{r},\omega) = \int d\mathbf{r}' \chi(\mathbf{r},\mathbf{r}',\omega)\mathbf{E}_s(\mathbf{r}',\omega) , \tag{2.1}$$

where $\mathbf{E}_s$ is the transverse part of the Maxwell electric field $\mathbf{E}$:

$$\mathbf{E}_s(\mathbf{r},\omega) = \frac{i\omega}{c}\mathbf{A}(\mathbf{r},\omega) = \mathbf{E}(\mathbf{r},\omega) - \mathbf{E}_{\mathrm{dep}}(\mathbf{r},\omega) , \tag{2.2}$$

$$\mathbf{E}_{\mathrm{dep}}(\mathbf{r},\omega) = \mathrm{grad}\,\mathrm{div} \int d\mathbf{r}' \frac{1}{|\mathbf{r}-\mathbf{r}'|}\mathbf{P}(\mathbf{r}',\omega) , \tag{2.3}$$

and

$$\chi(\mathbf{r},\mathbf{r}',\omega)=\sum_{\lambda}\left(\frac{\boldsymbol{\rho}_{\lambda}(\mathbf{r})^{*}\boldsymbol{\rho}_{\lambda}(\mathbf{r}')}{E_{\lambda}-\hbar\omega-i\gamma_{\lambda}}+\frac{\boldsymbol{\rho}_{\lambda}(\mathbf{r})\boldsymbol{\rho}_{\lambda}(\mathbf{r}')^{*}}{E_{\lambda}+\hbar\omega+i\gamma_{\lambda}}\right)+\sum_{\xi\eta}\chi_{\xi\eta}^{(b)}\hat{\mathbf{e}}_{\xi}\hat{\mathbf{e}}_{\eta}\delta(\mathbf{r}-\mathbf{r}')\tilde{\theta}(\mathbf{r})\tilde{\theta}(\mathbf{r}')\ . \quad (2.4)$$

The $\boldsymbol{\rho}_{\lambda}(\mathbf{r})$ is the transition dipole density between the ground state and the state λ with excitation energy E_{λ}. It should be noted that the material Hamiltonian is defined to contain the full (instantaneous) Coulomb interactions among charged particles. The electronic system is assumed to be in the ground state in the remote past, and the interaction with light is switched on adiabatically ($\gamma_{\lambda}=0^{+}$). We have neglected the quadratic term of $\mathbf{A}$ in the Hamiltonian, since we are considering linear response. We have also neglected the linear term of $\mathbf{A}$ in the expression of the current density, since the resonant effect is our concern. If we retain this linear term, it can be shown that the term yields factors $(\hbar\omega/E_{\lambda})$ and $-(\hbar\omega/E_{\lambda})$ for the resonant and antiresonant terms, respectively. It should be noted that the factor $(\hbar\omega/E_{\lambda})$ is almost equal to unity at the resonance condition. Though there appears an extra factor -1 for the antiresonant terms, they are negligible as far as we investigate the resonant structures. The neglected terms will be included in future work, in which we generalize the present theory together with the extension to nonlinear responses.

The last term of Eq. (2.4) is attached to take account of neglected degrees of freedom in the form of the background susceptibility. The $\hat{\mathbf{e}}_{\xi}$ is the unit vector pointing to the ξ axis ($\xi=x,y,z$) and $\tilde{\theta}$ is unity in the region which the matter fills, and is zero elsewhere. Although we introduce the background susceptibility, the formulation can be applied almost in parallel with the case without it.[4] By expanding the δ function in terms of a complete set, $\{\varphi_i\}$, as

$$\delta(\mathbf{r}-\mathbf{r}')=\sum_{i}\varphi_{i}(\mathbf{r})\varphi_{i}^{*}(\mathbf{r}')\ , \quad (2.5)$$

the "separable" property of $\chi(\mathbf{r},\mathbf{r}',\omega)$ is preserved. The solution of the Maxwell equations with the polarization as a source term is given as

$$\mathbf{E}(\mathbf{r},\omega)=\mathbf{E}_{0}(\mathbf{r},\omega)+\mathbf{E}_{r}(\mathbf{r},\omega)\ , \quad (2.6)$$

where $\mathbf{E}_{0}$ is the incident field (the homogeneous term) and the inhomogeneous term $\mathbf{E}_{r}$ is given as

$$\mathbf{E}_{r}(\mathbf{r},\omega)=(q^{2}+\text{grad div})\int d\mathbf{r}'\frac{e^{iq|\mathbf{r}-\mathbf{r}'|}}{|\mathbf{r}-\mathbf{r}'|}\mathbf{P}(\mathbf{r}',\omega)\ , \quad (2.7)$$

$$\left(q=\frac{\omega}{c}\right)\ .$$

Combining Eqs. (2.1) and (2.6) and making use of the separability of χ, we get

$$\mathbf{P}(\mathbf{r},\omega)=\sum_{\lambda}[F_{\lambda}\boldsymbol{\rho}_{\lambda}^{*}(\mathbf{r})+\tilde{F}_{\lambda}\boldsymbol{\rho}_{\lambda}(\mathbf{r})]+\sum_{i\xi}G_{i\xi}\boldsymbol{\varphi}_{i\xi}(\mathbf{r})\ , \quad (2.8)$$

where

$$\boldsymbol{\varphi}_{i\xi}(\mathbf{r})\equiv\tilde{\theta}(\mathbf{r})\varphi_{i}(\mathbf{r})\hat{\mathbf{e}}_{\xi}\ . \quad (2.9)$$

The coefficients F, $\tilde{F}$, and G are defined as

$$F_{\lambda}=(E_{\lambda}-\hbar\omega-i\gamma_{\lambda})^{-1}\int d\mathbf{r}\boldsymbol{\rho}_{\lambda}(\mathbf{r})\cdot\mathbf{E}_{s}(\mathbf{r}), \quad (2.10)$$

$$\tilde{F}_{\lambda}=(E_{\lambda}+\hbar\omega+i\gamma_{\lambda})^{-1}\int d\mathbf{r}\boldsymbol{\rho}_{\lambda}^{*}(\mathbf{r})\cdot\mathbf{E}_{s}(\mathbf{r}), \quad (2.11)$$

$$G_{i\xi}=\sum_{\eta}\chi_{\xi\eta}^{(b)}\int d\mathbf{r}\boldsymbol{\varphi}_{i\eta}^{*}(\mathbf{r})\cdot\mathbf{E}_{s}(\mathbf{r})\ . \quad (2.12)$$

The self-consistent equations (2.1) and (2.6) for $\mathbf{E}(\mathbf{r},\omega)$ and $\mathbf{P}(\mathbf{r},\omega)$ are rewritten into a set of linear equations for F, $\tilde{F}$, and G as

$$(E_{\lambda}-\hbar\omega-i\gamma_{\lambda})F_{\lambda}-\sum_{\mu}[A_{\lambda\mu}F_{\mu}+\tilde{A}_{\lambda\mu}\tilde{F}_{\mu}]-\sum_{i\xi}B_{\lambda,i\xi}G_{i\xi}=c_{\lambda}^{(0)}, \quad (2.13a)$$

$$(E_{\lambda}+\hbar\omega+i\gamma_{\lambda})\tilde{c}_{\lambda}-\sum_{\mu}[A'_{\lambda\mu}\tilde{F}_{\mu}+\tilde{A}'_{\lambda\mu}F_{\mu}]-\sum_{i\xi}\tilde{B}_{\lambda,i\xi}G_{i\xi}=\tilde{c}_{\lambda}^{(0)}\ , \quad (2.13b)$$

$$\sum_{\eta}(\chi^{(b)-1})_{\xi\eta}G_{i\eta}-\sum_{j\eta}C_{i\xi,j\eta}G_{j\eta}-\sum_{\mu}(B'_{i\xi,\mu}F_{\mu}+\tilde{B}'_{i\xi,\mu}\tilde{F}_{\mu})=d_{i\xi}^{(0)}\ , \quad (2.13c)$$

where

$$\begin{aligned}
A_{\lambda\mu}&=\mathcal{R}[\boldsymbol{\rho}_{\lambda},\boldsymbol{\rho}_{\mu}^{*}]\ , & \tilde{A}_{\lambda\mu}&=\mathcal{R}[\boldsymbol{\rho}_{\lambda},\boldsymbol{\rho}_{\mu}]\ ,\\
A'_{\lambda\mu}&=\mathcal{R}[\boldsymbol{\rho}_{\lambda}^{*},\boldsymbol{\rho}_{\mu}]\ , & \tilde{A}'_{\lambda\mu}&=\mathcal{R}[\boldsymbol{\rho}_{\lambda}^{*},\boldsymbol{\rho}_{\mu}^{*}]\ ,\\
B_{\lambda,i\xi}&=\mathcal{R}[\boldsymbol{\rho}_{\lambda},\boldsymbol{\varphi}_{i\xi}]\ , & \tilde{B}_{\lambda,i\xi}&=\mathcal{R}[\boldsymbol{\rho}_{\lambda}^{*},\boldsymbol{\varphi}_{i\xi}]\ ,\\
B'_{i\xi,\lambda}&=\mathcal{R}[\boldsymbol{\varphi}_{i\xi}^{*},\boldsymbol{\rho}_{\lambda}^{*}]\ , & \tilde{B}'_{i\xi,\lambda}&=\mathcal{R}[\boldsymbol{\varphi}_{i\xi}^{*},\boldsymbol{\rho}_{\lambda}]\ ,\\
C_{i\xi,j\eta}&=\mathcal{R}[\boldsymbol{\varphi}_{i\xi}^{*},\boldsymbol{\varphi}_{j\eta}]\ , & &
\end{aligned} \quad (2.14)$$

with

$$\mathcal{R}[\boldsymbol{\rho}_{\lambda},\boldsymbol{\rho}_{\mu}]\equiv\iint d\mathbf{r}d\mathbf{r}'\left(\boldsymbol{\rho}_{\lambda}(\mathbf{r})\cdot\boldsymbol{\rho}_{\mu}(\mathbf{r}')\frac{q^{2}e^{iq|\mathbf{r}-\mathbf{r}'|}}{|\mathbf{r}-\mathbf{r}'|}-\text{div}\boldsymbol{\rho}_{\lambda}(\mathbf{r})\text{div}\boldsymbol{\rho}_{\mu}(\mathbf{r}')\frac{e^{iq|\mathbf{r}-\mathbf{r}'|}-1}{|\mathbf{r}-\mathbf{r}'|}\right)\ , \quad (2.15)$$

and

$$c_\lambda^{(0)} = \int \boldsymbol{\rho}_\lambda(\mathbf{r}) \cdot \mathbf{E}_0(\mathbf{r}) d\mathbf{r} \ , \tag{2.16a}$$

$$\tilde{c}_\lambda^{(0)} = \int \boldsymbol{\rho}_\lambda^*(\mathbf{r}) \cdot \mathbf{E}_0(\mathbf{r}) d\mathbf{r} \ , \tag{2.16b}$$

$$d_{i\xi}^{(0)} = \int \boldsymbol{\varphi}_{i\xi}^*(\mathbf{r}) \cdot \mathbf{E}_0(\mathbf{r}) d\mathbf{r} \ . \tag{2.16c}$$

It should be noted that $\mathcal{R}$ represents the retarded interaction among induced dipoles via photons, while all the information of the incident field are included in $c^{(0)}$'s, $\tilde{c}^{(0)}$'s, and $d^{(0)}$'s on the right hand side of the equations. Equations (2.13a)–(2.13c) may be written in a matrix form,

$$\begin{pmatrix} & S & \end{pmatrix} \begin{pmatrix} F \\ \tilde{F} \\ G \end{pmatrix} = \begin{pmatrix} c^{(0)} \\ \tilde{c}^{(0)} \\ d^{(0)} \end{pmatrix} \ . \tag{2.17}$$

The resonant frequency is determined by the zeros of the determinant of the coefficient matrix (S), which contains $\mathcal{R}$. This is the same condition for the existence of nontrivial solutions of $(F, \tilde{F}, G)$ in the absence of the incident field ($c_\lambda^{(0)} = \tilde{c}_\lambda^{(0)} = d_{i\xi}^{(0)} = 0$). The energy correction, due to the retarded interaction, has generally a complex value. The imaginary part of the correction gives the spontaneous emission rate.

With the use of the Fourier transform, $\mathcal{R}$ may be expressed as

$$\mathcal{R}[\boldsymbol{\rho}_\lambda, \boldsymbol{\rho}_\mu] = \frac{1}{4\pi^2} \int d\mathbf{k} \left\{ \frac{1}{k} \left(\frac{1}{k - q - i\epsilon} + \frac{1}{k + q + i\epsilon} \right) \left[q^2 \tilde{\boldsymbol{\rho}}_\lambda(\mathbf{k}) \cdot \tilde{\boldsymbol{\rho}}_\mu(-\mathbf{k}) - [\tilde{\boldsymbol{\rho}}_\lambda(\mathbf{k}) \cdot \mathbf{k}][\tilde{\boldsymbol{\rho}}_\mu(-\mathbf{k}) \cdot \mathbf{k}] \right] \right.$$
$$\left. + \frac{1}{k} \left(\frac{1}{k - i\epsilon} + \frac{1}{k + i\epsilon} \right) [\tilde{\boldsymbol{\rho}}_\lambda(\mathbf{k}) \cdot \mathbf{k}][\tilde{\boldsymbol{\rho}}_\mu(-\mathbf{k}) \cdot \mathbf{k}] \right\} , \tag{2.18}$$

where

$$\tilde{\boldsymbol{\rho}}_\lambda(\mathbf{k}) = \int d\mathbf{r} \boldsymbol{\rho}_\lambda(\mathbf{r}) e^{i\mathbf{k}\cdot\mathbf{r}} \ , \tag{2.19}$$

with $k = |\mathbf{k}|$ and $\epsilon = 0^+$. The behavior of $\tilde{\boldsymbol{\rho}}_\lambda(\mathbf{k})$ at $|\mathbf{k}| \to \infty$ is important to give a finite retarded interaction. Point dipole approximation for $\boldsymbol{\rho}_\lambda(\mathbf{r})$ yields ultraviolet divergence in Eq. (2.18).

The solution (2.7) with (2.8) gives the response field at any position $\mathbf{r}$. At a point far from the matter ($|\mathbf{r}| \to \infty$), the response field has an asymptotic form as

$$\mathbf{E}_r(\mathbf{r}) \sim \frac{e^{iqr}}{r} \left(\sum_\lambda \left\{ F_\lambda [q^2 \tilde{\boldsymbol{\rho}}_\lambda^*(\mathbf{q}) - \mathbf{q}\mathbf{q} \cdot \tilde{\boldsymbol{\rho}}_\lambda^*(\mathbf{q})] \right.\right.$$
$$\left. + \tilde{F}_\lambda [q^2 \tilde{\boldsymbol{\rho}}_\lambda(-\mathbf{q}) - \mathbf{q}\mathbf{q} \cdot \tilde{\boldsymbol{\rho}}_\lambda(-\mathbf{q})] \right\}$$
$$\left. + \sum_{i\xi} G_{i\xi} [q^2 \tilde{\boldsymbol{\varphi}}_{i\xi}(-\mathbf{q}) - \mathbf{q}\mathbf{q} \cdot \tilde{\boldsymbol{\varphi}}_{i\xi}(-\mathbf{q})] \right) , \tag{2.20}$$

with $\mathbf{q} = q\mathbf{r}/r$. The quantity inside the outermost brackets depends only on the angle but not on the distance. The response spectra to be calculated later is its absolute square. When the matter system is small compared with the wavelength $\lambda = 2\pi/q$, the leading term of $\tilde{\boldsymbol{\rho}}_\lambda(\mathbf{k})$ is $\mathbf{k}$ independent and $\tilde{\boldsymbol{\rho}}_\lambda(0)$ is a vector associated with the λth excited state. Then $\mathbf{E}_r(\mathbf{r})$ is the superposition of the dipole patterns of all $\tilde{\boldsymbol{\rho}}_\lambda(0)$ and $\tilde{\boldsymbol{\varphi}}_{i\xi}(0)$. When the system is large, the $\mathbf{k}$ dependence of $\tilde{\boldsymbol{\rho}}$ becomes important, which produces an extra angle dependence of $\mathbf{E}_r$ at $r \to \infty$. From Eq. (2.18), we see that the retarded interaction also follows this criterion. Thus, the response of the systems is expected to change according to the system size in comparison with the wavelength λ.

Although the above formulation will generally be used in the numerical calculation of response spectra, only the part of the equations containing the matrix A dominates the resonant structures. In particular, when the resonant energies are well separated from one another or when the off-diagonal elements of the matrix S are small, the self-energy correction to E_λ is determined mainly by $-A_{\lambda\lambda}$. It will be shown that the response spectra in resonant ranges are reproduced by the diagonal elements of A at least for the parameter values and geometry used in the numerical study.

III. MODEL

We consider D-dimensional lattices with a lattice spacing b of semiconductor spheres. The b is taken to be much smaller than the wavelength of resonant light so that the system may be either microscopic and macroscopic depending on the number of the spheres. It is assumed that each sphere is so small that the level separation due to size quantization of the exciton center-of-mass (CM) motion is quite large and thereby a degenerate two level model may be adopted to describe the resonant structure of each sphere. We also assume that the radius of the $1s$-type relative motion is so small like in CuCl, in which the radius is about 7 Å, that the transition current densities reflect the detail of the CM wave functions alone. Then the transition dipole densities for each sphere are expressed as[15]

$$\boldsymbol{\rho}_{m\xi}^0(\mathbf{r}) = \hat{\boldsymbol{\rho}}_\xi^0 N_0 j_0(k_0|\mathbf{r} - \mathbf{r}_m|) \theta(R - |\mathbf{r} - \mathbf{r}_m|) \ ,$$
$$\left(N_0 = \sqrt{\frac{\pi}{2R^3}} \right) \ , \tag{3.1}$$

where R is the radius of the sphere, $\mathbf{r}_m$ is the center of the mth sphere, θ is the Heaviside function and ξ refers to the degenerate excitation levels with the transition dipole moments directed to the x, y, and z axes. The k_0 is determined by the size-quantization condition, $j_0(k_0R) = 0$, i.e., $k_0R = \pi$. The amplitude of $\hat{\boldsymbol{\rho}}^0_\xi$ is related to the longitudinal and transverse splitting $\Delta_{\rm LT}$ in the bulk crystal as

$$|\hat{\boldsymbol{\rho}}^0_\xi|^2 = \frac{\Delta_{\rm LT}}{4\pi}\epsilon_b \ , \tag{3.2}$$

where ϵ_b is the background dielectric constant. The resonant energy E_p of an isolated particle is given as the sum of the bulk excitation energy E_b, the size-quantization energy $E_{\rm sq} = (\hbar k_0)^2/2M$, and the depolarization shift $E_{\rm dep} = \Delta_{\rm LT}/4\pi$ inside the sphere,[16] where M is the mass of the exciton. It is assumed that the charge transfer does not occur among the spheres, but the excitation itself can hop like a Frenkel exciton, due to the dipole-dipole interaction included in the material Hamiltonian. Thus the transition dipole density for the λth excited state is written as a linear combination of $\boldsymbol{\rho}^0_{m\xi}$:

$$\boldsymbol{\rho}_\lambda(\mathbf{r}) = \sum_{m\xi} w_{\lambda m\xi}\boldsymbol{\rho}^0_{m\xi}(\mathbf{r}) \ , \tag{3.3}$$

where $w_{\lambda m\xi}$ and the corresponding excitation energy are determined by

$$\sum_{n\eta} t_{m\xi;n\eta}w_{\lambda n\eta} = E_\lambda w_{\lambda m\xi} \ , \tag{3.4}$$

with

$$t_{m\xi;m\eta} = E_p\delta_{\xi\eta} \ , \tag{3.5}$$

$$t_{m\xi;n\eta} = \frac{1}{r^3_{mn}}\left[(\boldsymbol{\mu}_\xi\cdot\boldsymbol{\mu}_\eta) - 3(\boldsymbol{\mu}_\xi\cdot\hat{\mathbf{r}}_{mn})(\boldsymbol{\mu}_\eta\cdot\hat{\mathbf{r}}_{mn})\right] \ , \quad (m\neq n) \tag{3.6}$$

$$(\mathbf{r}_{mn} = \mathbf{r}_m - \mathbf{r}_n \ , r_{mn} = |\mathbf{r}_{mn}| \ , \hat{\mathbf{r}}_{mn} = \mathbf{r}_{mn}/r_{mn}) \ ,$$

$$\boldsymbol{\mu}_\xi = \int d\mathbf{r}\boldsymbol{\rho}^0_{m\xi} = N_0\hat{\boldsymbol{\rho}}^0_\xi\frac{4R^3}{\pi} \quad (\propto R^{3/2}) \ . \tag{3.7}$$

It should be noted that w's form a complete set;

$$\sum_\lambda w_{\lambda m\xi}w^*_{\lambda n\eta} = \delta_{mn}\delta_{\xi\eta}. \tag{3.8}$$

This will be used to derive a sum rule of A.

The background susceptibility $\chi^{(b)}$ is assumed to be isotropic;

$$\chi^{(b)}_{\xi\eta} = \chi_b\delta_{\xi\eta} \ . \tag{3.9}$$

The final approximation is concerned with $\{\varphi_i\}$. We replace it by $\{\theta(R-|\mathbf{r}-\mathbf{r}_m|)\}$. Since the approximation is made to the background susceptibility of a sphere, this is related to the well-known Mie theory. A criterion for the maximum angular momentum $\ell_{\rm MAX}$ has been given for the Mie theory as follows.[17] The value of $\ell_{\rm MAX}$ is the integer closest to $x + 4x^{1/3} + 1$, where $x = R/\lambda$.[18] For the parameters used in our paper, $\ell_{\rm MAX}$ becomes 2. Our coarse graining seems rather rough. However, because we are discussing the resonant structure of mesoscopic systems, the contribution from the background susceptibility is of secondary importance. We have checked this by discarding some terms including the contribution from the background susceptibility when we calculate the response spectra. (See the explanation of Fig. 3 in the text.) Therefore, we believe that the approximation will not change the results given in this paper. For more general cases, the above criterion must be considered.

In the following, we will consider a linear chain, a planar system (a square lattice) and a simple cubic system of the spheres. For simplicity of the description, we assume that the chain lies along the z axis. In the linear chain, the dipole moments pointing to the x, y, and z axes, have no mutual dipole-dipole and retarded interactions, due to the geometrical reason, and they can be treated independently. In the planar system, the dipole moments perpendicular to the plane also can be considered separately from those lying in the plane. The dipole moments in the plane in finite planar systems and those in finite cubic systems can no longer be decoupled, while they can be further decoupled in infinite systems (because of the translational invariance as will be seen later). Actually, this coupling will be seen to lead to a complex behavior of the size dependence of the matrix A in $D = 2$ and 3.

IV. ANALYTIC EXPRESSION OF A

We investigate the matrix elements of S analytically within the present model. Only A is considered here, since it dominates the energy correction and the others can be calculated similarly. Expanding $\boldsymbol{\rho}_\lambda(\mathbf{r})$ in terms of $\boldsymbol{\rho}^0_{m\xi}(\mathbf{r})$ as in Eq. (3.3), we have

$$A_{\lambda\mu} = \sum_{mn,\xi\eta} w_{\lambda m\xi}w^*_{\mu n\eta}\mathcal{A}_{m\xi,n\eta} \ . \tag{4.1}$$

The integration inside the spheres in $\mathcal{A}_{m\xi,n\eta} = \mathcal{R}[\boldsymbol{\rho}^0_{m\xi},\boldsymbol{\rho}^{0*}_{n\eta}]$ yields the explicit form as

$$\mathcal{A}_{m\xi,n\eta} = q^2\frac{e^{iqr_{mn}}}{r_{mn}}V_s^2(qR)\left\{\boldsymbol{\mu}_\xi\cdot\boldsymbol{\mu}^*_\eta - (\boldsymbol{\mu}_\xi\cdot\hat{\mathbf{r}}_{mn})(\boldsymbol{\mu}^*_\eta\cdot\hat{\mathbf{r}}_{mn}) - \frac{1-iqr_{mn}}{q^2r^2_{mn}}\left[\boldsymbol{\mu}_\xi\cdot\boldsymbol{\mu}^*_\eta - 3(\boldsymbol{\mu}_\xi\cdot\hat{\mathbf{r}}_{mn})(\boldsymbol{\mu}^*_\eta\cdot\hat{\mathbf{r}}_{mn})\right]\right\}$$

$$+\frac{1}{r^3_{mn}}\left[\boldsymbol{\mu}_\xi\cdot\boldsymbol{\mu}^*_\eta - 3(\boldsymbol{\mu}_\xi\cdot\hat{\mathbf{r}}_{mn})(\boldsymbol{\mu}^*_\eta\cdot\hat{\mathbf{r}}_{mn})\right] \quad (\text{for } \mathbf{r}_m\neq\mathbf{r}_n) \ , \tag{4.2}$$

$$\mathcal{A}_{m\xi,m\eta} = \boldsymbol{\mu}_\xi \cdot \boldsymbol{\mu}_\eta^* \frac{2q^2}{3R} \frac{\pi^2}{\pi^2 - (qR)^2} \left(e^{iqR} V_s(qR) + \frac{1}{2} \right) \quad (\text{for } \mathbf{r}_m = \mathbf{r}_n) , \tag{4.3}$$

where

$$V_s(X) = \frac{\sin X}{X} \frac{\pi^2}{\pi^2 - X^2} . \tag{4.4}$$

For general cases, the use of the Fourier transform is also convenient. Putting

$$\tilde{\boldsymbol{\rho}}^0_{m\xi}(\mathbf{k}) \equiv \int d\mathbf{r} \boldsymbol{\rho}^0_{m\xi}(\mathbf{r}) e^{i\mathbf{k}\cdot\mathbf{r}} = \boldsymbol{\mu}_\xi V_s(kR) e^{i\mathbf{k}\cdot\mathbf{r}_m} , \tag{4.5}$$

into Eq. (2.18), we have

$$\mathcal{A}_{m\xi,n\eta} = \int d\mathbf{k} e^{i\mathbf{k}\cdot\mathbf{r}_{mn}} \tilde{\mathcal{A}}_{\xi\eta}(\mathbf{k}) , \tag{4.6}$$

$$\begin{aligned} \tilde{\mathcal{A}}_{\xi\eta}(\mathbf{k}) = \frac{1}{4\pi^2} V_s^2(kR) \Bigg\{ & \frac{1}{k} \left(\frac{1}{k - q - i\epsilon} + \frac{1}{k + q + i\epsilon} \right) \\ & \times [q^2 \boldsymbol{\mu}_\xi \cdot \boldsymbol{\mu}_\eta^* - (\boldsymbol{\mu}_\xi \cdot \mathbf{k})(\boldsymbol{\mu}_\eta^* \cdot \mathbf{k})] \\ & + \frac{1}{k} \left(\frac{1}{k - i\epsilon} + \frac{1}{k + i\epsilon} \right) (\boldsymbol{\mu}_\xi \cdot \mathbf{k})(\boldsymbol{\mu}_\eta^* \cdot \mathbf{k}) \Bigg\} . \end{aligned} \tag{4.7}$$

Equation (4.1) may be written as

$$A_{\lambda\mu} = \sum_{\xi\eta} \int d\mathbf{k} \tilde{w}_{\lambda\xi}(\mathbf{k}) \tilde{w}^*_{\mu\eta}(\mathbf{k}) \tilde{\mathcal{A}}_{\xi\eta}(\mathbf{k}) , \tag{4.8}$$

with

$$\tilde{w}_{\lambda\xi}(\mathbf{k}) = \sum_m e^{i\mathbf{k}\cdot\mathbf{r}_m} w_{\lambda m\xi} . \tag{4.9}$$

For the finite D-dimensional array in question, we consider the corresponding periodic lattice by allowing $\mathbf{r}_m$ to be extended infinitely in the D dimension. Let us define $\mathbf{k}_\parallel$ as the component of $\mathbf{k}$ describing the periodicity of the D-dimensional lattice, and the corresponding reciprocal lattice vectors are denoted as $\{\mathbf{g}\}$. Then, it is clear that $\tilde{w}_{\lambda\xi}$, being a function of $\mathbf{k}_\parallel$, satisfies

$$\tilde{w}_{\lambda\xi}(\mathbf{k}_\parallel + \mathbf{g}) = \tilde{w}_{\lambda\xi}(\mathbf{k}_\parallel) . \tag{4.10}$$

Denoting the remaining component of $\mathbf{k}$ as $\mathbf{k}_\perp$, we can rewrite Eq. (4.8) as

$$\begin{aligned} A_{\lambda\mu} = & \sum_{\xi\eta} \int_{\mathrm{BZ}} d\mathbf{k}_\parallel \tilde{w}_{\lambda\xi}(\mathbf{k}_\parallel) \tilde{w}^*_{\mu\eta}(\mathbf{k}_\parallel) \\ & \times \sum_{\mathbf{g}} \int d\mathbf{k}_\perp \tilde{\mathcal{A}}_{\xi\eta}(\mathbf{k})|_{\mathbf{k}=\mathbf{k}_\parallel+\mathbf{g}+\mathbf{k}_\perp} , \end{aligned} \tag{4.11}$$

where the integration over $\mathbf{k}_\parallel$ is carried out in the first Brillouin zone of the infinite system. For $D = 3$, $\mathbf{k}_\parallel$ is three dimensional and the integration over $\mathbf{k}_\perp$ is omitted.

For infinite lattices, because of the translational invariance, we have

$$w_{\lambda m\xi} = \frac{1}{N^{D/2}} \hat{w}_{\lambda\xi} e^{i\mathbf{k}_\lambda \cdot \mathbf{r}_m} , \tag{4.12}$$

which allows us to perform the lattice sum in Eq. (4.1) or (4.9). Here, $\mathbf{k}_\lambda$ is a wave vector in the D-dimensional Brillouin zone. We conventionally introduced the number of the lattice points, N^D, and take the limit $N \to \infty$ after the lattice summation is carried out. From Eqs. (4.9), (4.11), and (4.12), we obtain

$$\begin{aligned} A_{\lambda\mu} = & \delta_{\mathbf{k}_\lambda \mathbf{k}_\mu} \sum_{\xi\eta} \hat{w}_{\lambda\xi} \hat{w}^*_{\mu\eta} \left(\frac{2\pi}{b} \right)^D \\ & \times \sum_{\mathbf{g}} \delta_{\mathbf{k}_\lambda + \mathbf{k}_\parallel, \mathbf{g}} \int d\mathbf{k}_\perp \tilde{\mathcal{A}}_{\xi\eta}(\mathbf{k}) \Big|_{\mathbf{k}^2 = \mathbf{k}_\parallel^2 + \mathbf{k}_\perp^2} . \end{aligned} \tag{4.13}$$

In the periodic systems, the ultraviolet divergence of $A_{\lambda\mu}$ for a point dipole mentioned in Sec. II appears in the integration over $\mathbf{k}_\perp$ and in the sum over $\mathbf{g}$ for $D = 1$ and $D = 2$, respectively. For finite extension of dipole density $\boldsymbol{\rho}_\lambda(\mathbf{r})$, this divergence is suppressed by $V_s(kR)^2$ in $\tilde{A}_{\xi\eta}(\mathbf{k})$.

For simplicity in the following, we define

$$k_\lambda = |\mathbf{k}_\lambda| , \tag{4.14}$$

$$\hat{\mathbf{k}}_\lambda = \mathbf{k}_\lambda / k_\lambda . \tag{4.15}$$

We also define, for a later use,

$$\hat{\boldsymbol{\mu}}_\lambda = \sum_\xi \hat{w}_{\lambda\xi} \boldsymbol{\mu}_\xi . \tag{4.16}$$

The $\hat{\boldsymbol{\mu}}_\lambda$'s are either parallel or perpendicular to $\mathbf{k}_\lambda$, and the two perpendicular ones with the same $\mathbf{k}_\lambda$'s are perpendicular to each other by virtue of the dipole interaction (and by orthogonalizing them if they are degenerate.) Therefore, $\hat{\boldsymbol{\mu}}_\lambda$'s corresponding to the same $\mathbf{k}_\lambda$ are perpendicular to one another. We will see that A is diagonal in infinite systems because of this fact.

A. Zero-dimensional case

For a single sphere, Eq. (4.3) gives $A_{\xi\eta}$ itself;

$$A^{(0)}_{\xi\eta} = \boldsymbol{\mu}_\xi \cdot \boldsymbol{\mu}_\eta^* \frac{2q^2}{3R} \frac{\pi^2}{\pi^2 - (qR)^2} \left(e^{iqR} V_s(qR) + \frac{1}{2} \right) . \tag{4.17}$$

By the LWA ($qR \ll 1$), we have

$$A^{(0)}_{\xi\eta} \sim \mu^2 \delta_{\xi\eta} \left(\frac{q^2}{R} + i\frac{2}{3}q^3 \right) , \tag{4.18}$$

where we have used $\boldsymbol{\mu}_\xi \cdot \boldsymbol{\mu}_\eta = \mu^2 \delta_{\xi\eta}$. The imaginary part of $A^{(0)}_{\xi\xi}$ is the well-known formula of the spontaneous decay width in QED and has apparent linear dependence on the volume through μ^2 [see Eq. (3.7)].

B. One-dimensional periodic case

Evaluation of the sums over m and n in Eq. (4.1) with Eqs. (4.2), (4.3), and (4.12) can be done analytically. Appendix B gives the result, which is valid even for $qb > 1$. The resonant wavelength is, however, much larger than the lattice constant for the present geometry and resonant energy. Assuming $0 < q < \pi/b$, we have

$$\begin{aligned} A^{(1)}_{\lambda\mu} = \delta_{\mathbf{k}_\lambda \mathbf{k}_\mu} \Bigg[& \hat{\boldsymbol{\mu}}_\lambda \cdot \hat{\boldsymbol{\mu}}^*_\mu \frac{2q^2}{3R} \frac{\pi^2}{\pi^2 - (qR)^2} \left(\cos(qR) V_s(qR) + \frac{1}{2} \right) \\ & + V_s(qR)^2 \Bigg[-I^{(1)} \ln |\cos qb - \cos k_\lambda b| - 2\frac{q^2}{b} (\hat{\boldsymbol{\mu}}_\lambda \cdot \hat{\mathbf{k}}_\lambda)(\hat{\boldsymbol{\mu}}_\mu \cdot \hat{\mathbf{k}}_\mu) \ln 2 \\ & + I^{(3)} \left(\int_0^{k_\lambda b - qb} dt (k_\lambda b - t) \ln \left| \sin \frac{t}{2} \right| + \int_0^{k_\lambda b + qb} dt (k_\lambda b - t) \ln \sin \frac{t}{2} + 2\zeta(3) + k_\lambda^2 b^2 \ln 2 \right) \\ & + i\pi\theta(q - k_\lambda) \frac{1}{2b} \left\{ q^2 \left[\hat{\boldsymbol{\mu}}_\lambda \cdot \hat{\boldsymbol{\mu}}^*_\mu + (\hat{\mathbf{k}}_\lambda \cdot \hat{\boldsymbol{\mu}}_\lambda)(\hat{\mathbf{k}}_\mu \cdot \hat{\boldsymbol{\mu}}^*_\mu) \right] + k_\lambda^2 \left[\hat{\boldsymbol{\mu}}_\lambda \cdot \hat{\boldsymbol{\mu}}^*_\mu - 3(\hat{\mathbf{k}}_\lambda \cdot \hat{\boldsymbol{\mu}}_\lambda)(\hat{\mathbf{k}}_\mu \cdot \hat{\boldsymbol{\mu}}^*_\mu) \right] \right\} \Bigg] \\ & - I^{(3)} \left(2 \int_0^{k_\lambda b} dt (k_\lambda b - t) \ln \sin \frac{t}{2} + 2\zeta(3) + k_\lambda^2 b^2 \ln 2 \right) \Bigg] , \end{aligned} \tag{4.19}$$

where I_ℓ's are given in Appendix B. A finite imaginary part appears for $k_\lambda < q$. This is a general matching condition of the wave vectors for matter states and radiation states. Only for $k_\lambda < q$, there occurs a coupling between the matter states and the propagating light states, which leads to the radiative decay of the former. Dipole density with $k_\lambda > q$ emits only evanescent electromagnetic waves. It is recognized that the argument of the absolute values in the first and third terms in the curly brackets are negative for $k_\lambda < q$ and their logarithms yield the imaginary part. For $qb, k_\lambda b \ll 1$, Eq. (4.19) is reduced to

$$\begin{aligned} A^{(1)}_{\lambda\mu} = -\delta_{\lambda\mu} \frac{\mu^2}{2b} \Bigg\{ & \left(q^2(1 + \cos^2\varphi) + k_\lambda^2 (1 - 3\cos^2\varphi) \right) \\ & \times \left(\ln |q^2 - k_\lambda^2| b^2 - i\pi\theta(q - k_\lambda) \right) \\ & - (1 - 3\cos^2\varphi) k_\lambda^2 \ln(k_\lambda b)^2 - 2q^2 \frac{b}{R} \Bigg\} , \end{aligned} \tag{4.20}$$

where we have used the orthogonality of $\hat{\boldsymbol{\mu}}_\lambda$'s mentioned below Eq. (4.16) and φ is defined by $\boldsymbol{\mu}_\lambda \cdot \mathbf{k}_\lambda = \mu k_\lambda \cos\varphi$. (In the present model, φ is 0 or $\pi/2$.) The final result is almost the same as that of Orrit, Aslangul, and Kottis.[9] A small difference comes partly from the fact that they have ignored the size of the molecule but introduced cutoff by multiplying a Lorentzian to the integrand.

C. Two-dimensional periodic case

For the infinite layer, from Eq. (4.13), we have[19]

$$\begin{aligned} A^{(2)}_{\lambda\mu} = \delta_{\mathbf{k}_\lambda \mathbf{k}_\mu} \frac{2\pi}{b^2} \Bigg\{ & \frac{1}{\sqrt{\mathbf{k}_\parallel^2 - q^2}} \Big[q^2 \hat{\boldsymbol{\mu}}_{\lambda\parallel} \cdot \hat{\boldsymbol{\mu}}_{\mu\parallel} \\ & - (\hat{\boldsymbol{\mu}}_\lambda \cdot \mathbf{k}_\parallel)(\hat{\boldsymbol{\mu}}_\mu \cdot \mathbf{k}_\parallel) + k_\parallel^2 \hat{\boldsymbol{\mu}}_{\lambda\perp} \cdot \hat{\boldsymbol{\mu}}_{\mu\perp} \Big] \\ & + \frac{1}{k_\parallel} \Big[(\hat{\boldsymbol{\mu}}_\lambda \cdot \mathbf{k}_\parallel)(\hat{\boldsymbol{\mu}}_\mu \cdot \mathbf{k}_\parallel) \\ & - k_\parallel^2 \hat{\boldsymbol{\mu}}_{\lambda\perp} \cdot \hat{\boldsymbol{\mu}}_{\mu\perp} \Big] \Bigg\} \Bigg|_{\mathbf{k}_\parallel = \mathbf{k}_\lambda} , \end{aligned} \tag{4.21}$$

where $\hat{\boldsymbol{\mu}}_{\lambda\parallel}$ and $\hat{\boldsymbol{\mu}}_{\lambda\perp}$ are the components of $\hat{\boldsymbol{\mu}}_\lambda$ parallel and perpendicular to the two-dimensional plane, respectively, and $k_\parallel = |\mathbf{k}_\parallel|$. We have neglected the sum over nonzero $\mathbf{g}$ and $V_s(kR)$ because $V_s(kR)$ is very small for large k and is ~ 1 for $kR \ll 1$. Taking account of the orthogonality of $\boldsymbol{\mu}_\lambda$'s gives

$$\begin{aligned} A^{(2)}_{\lambda\mu} = \delta_{\lambda\mu} \frac{2\pi}{b^2} \Bigg\{ & \frac{1}{\sqrt{\mathbf{k}_\parallel^2 - q^2}} \left[q^2 \hat{\boldsymbol{\mu}}^2_{\lambda\parallel} - (\hat{\boldsymbol{\mu}}_\lambda \cdot \mathbf{k}_\parallel)^2 + k_\parallel^2 \hat{\boldsymbol{\mu}}^2_{\lambda\perp} \right] \\ & + \frac{1}{k_\parallel} \left[(\hat{\boldsymbol{\mu}}_\lambda \cdot \mathbf{k}_\parallel)^2 - k_\parallel^2 \hat{\boldsymbol{\mu}}^2_{\lambda\perp} \right] \Bigg\} \Bigg|_{\mathbf{k}_\parallel = \mathbf{k}_\lambda} . \end{aligned} \tag{4.22}$$

For $k_\parallel < q$, $\sqrt{k_\parallel^2 - q^2}$ corresponds to $-i\sqrt{q^2 - k_\parallel^2}$, which gives the imaginary part of A. The result is again the same as that of Orrit *et al.*[9] if we assume that $\hat{\boldsymbol{\mu}}_\lambda$'s lie in the plane.

D. Three-dimensional periodic case

For the infinite three-dimensional lattice, no integration remains and we have

$$A^{(3)}_{\lambda\mu} = \delta_{\mathbf{k}_\lambda \mathbf{k}_\mu} \frac{4\pi}{b^3} \sum_{\mathbf{g}} V_s^2(kR) \left\{ \frac{[q^2 \boldsymbol{\mu}_\lambda \cdot \boldsymbol{\mu}_\mu - (\mathbf{k}\cdot\boldsymbol{\mu}_\lambda)(\mathbf{k}\cdot\boldsymbol{\mu}_\mu)]}{k^2 - q^2} + \frac{(\mathbf{k}\cdot\boldsymbol{\mu}_\lambda)(\mathbf{k}\cdot\boldsymbol{\mu}_\mu)}{k^2} \right\} \Bigg|_{\mathbf{k}=\mathbf{g}-\mathbf{k}_\lambda} . \quad (4.23)$$

In this case, A has no finite imaginary part. The real part corresponds to the energy shift, due to the formation of "polariton," whose decay time is infinitely long. The disappearance of the radiative decay in the infinite three-dimensional lattice is due to the fact that the matter and light occupy the same space and there is no outside world to which light can escape. In other words, coupling to the radiative fields with infinite degrees of freedom is necessary to give rise to a finite lifetime. The experimentally observed radiative decay of polaritons in real crystals is due to the presence of surfaces on macroscopic samples.

In the following, we assume $q < \pi/b$ for simplicity. As seen above, the modes whose wave numbers are smaller than q have a finite imaginary energy shift $\Gamma^{(D)}$ for the lattices in $D = 1$ and 2. If we neglect $\mathbf{k}_\lambda$ dependence, we have

$$\Gamma^{(2)} \sim \frac{\pi}{qb}\Gamma^{(1)} \sim \frac{\pi^2}{(qb)^2}\Gamma^{(0)} . \quad (4.24)$$

In the present models, $1/qb$ can be quite large and this has been called an amplifying factor by Orrit *et al.*[9]

Putting Eq. (3.8) into Eq. (4.1), and forming the trace of A, we have

$$\mathrm{Tr}A = NN_L\mathcal{A}_{m\xi,m\xi} , \quad (4.25)$$

where N is the number of the spheres and N_L the number of the degrees of the freedom associated with the direction of dipole moment inside each sphere. (In the present model, $N_L = 3$.) This sum rule holds for both finite and infinite systems. If the dipole moments pointing to different axes are decoupled, the above identity holds for each decoupled set. When the off-diagonal elements vanish or are negligibly small, and therefore the (complex) radiative shift is determined by the diagonal elements, Eq. (4.25) means that the sum of the radiative shifts is the sum of those of the transition dipole moments of the individual sphere. This sum rule has important meaning especially for the imaginary part of the radiative shift (that is, radiative width) because its sign is positive for all the states. The amplifying factor may be considered as a consequence of the matching condition and the sum rule.

The transition dipole moment $\tilde{\boldsymbol{\rho}}_\lambda$ in the $\mathbf{k}$ space has a distribution with a width inversely proportional to the dimension of the system. The peak positions of the distribution are determined by the boundary condition. From the comparison of Eqs. (4.11) and (4.13), it is found that the $A_{\lambda\lambda}$ for a finite system is regarded as the weighted sum of the $A_{\lambda\lambda}$ for the corresponding infinite system in the same dimension, where the weighting factor is $|\tilde{w}_{\lambda\xi}(\mathbf{k}_\parallel)|^2$. Only the part of the distribution within the sphere of a radius q around the origin, $S^D(q)$, contributes to the radiative width. As the system size becomes large, the peaks approach to the origin and the widths become sharper. When the distribution begins to enter $S^D(q)$, the radiative width starts to grow. When the whole distribution of a given state λ has entered $S^D(q)$, the radiative shift becomes almost saturated. The radiative width is monopolized by a single mode only when the system is smaller than the wavelength of the resonant light. As we increase the system size, the modes with large radiative width appear and get saturated successively. This behavior is shown numerically in the next section.

V. NUMERICAL STUDY FOR FINITE SYSTEMS

Here we show numerical results for finite systems (assemblies of N spheres) and investigate the dependence of the response on the size N and the dimensionality D of the system. We consider a linear chain ($D = 1$), a square lattice ($D = 2$), and a simple cubic system ($D = 3$). We choose $R = 15$ Å and $b = 50$ Å as the parameters of the system size, and use $\Delta_{\mathrm{LT}} = 5.7$ meV, $E_b = 3.2041$ eV, and $\epsilon_b = 5.59$ for the particle's internal parameters. We set γ's to 0^+ so that the widths of the peaks in the response spectra are the net radiative decay widths.

A. $D = 1$

Since the dipole moments pointing to the x, y, and z axes are decoupled, we can treat them independently, as mentioned earlier. Due to the coupling of the excited states of the spheres via dipole-dipole interaction, there arises a set of discrete levels, which can be regarded as the size-quantized levels of the chain. The evolution of the response of these resonances as a function of N will be shown below.

Figure 1 shows the response spectra of the chains with small N's. The incident field comes perpendicularly to the chain with the polarization parallel to it. The responses are observed at the direction perpendicular to the chain and far from the chain so that only the dipole radiation component corresponding to Eq. (2.20) contributes. The peak in each frame corresponds to the lowest size-quantized level of the chain, which, in this geometry and size range, monopolizes the oscillator strength. The peak position is mainly determined by the dipole-dipole interaction, and in addition there is a slight shift due to radiative correction. The peak width, as expected, grows linearly with the size N in this size range.

Figure 2 shows similar spectra with larger N. The geometry is the same as in Fig. 1. Only main peaks are shown though other peaks with a narrower width appear in a higher energy range. The dash-dotted and the dashed lines show the energy levels, E_λ's, of the unperturbed Hamiltonian. Only the modes with even parity (shown by the dash-dotted lines) contribute the peaks under the geometry. [We refer to the parity according to the inversion symmetry of $w_{\lambda m\xi}$. The modes with odd

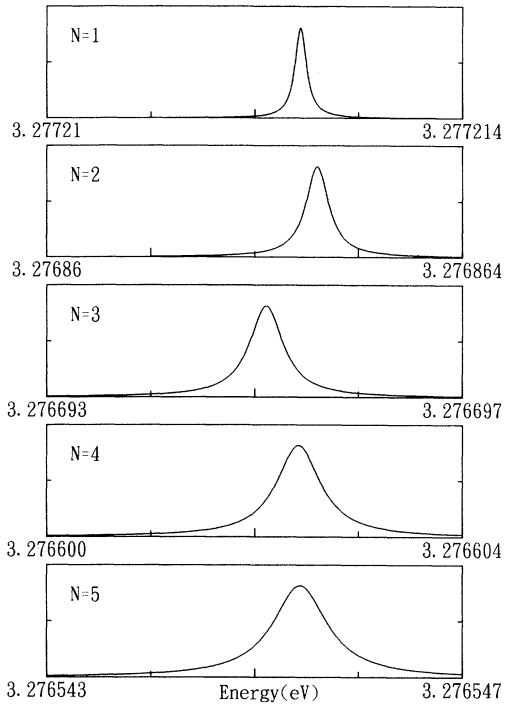

FIG. 1. The response spectra of the chains with small numbers of the spheres. The incident field is a plane wave propagating perpendicularly to the chain with the polarization parallel to it. The responses are observed at the direction perpendicular to the chain and far from it.

parity (shown by the dashed line) have no total transition dipole moment.] The peaks are shifted from them, due to the retarded interaction. The growth of the lowest peak width is almost saturated, while other peaks are becoming wider and approaching to the lowest one.

Figure 3 shows spectra for the chain with $N = 80$ observed in the direction at various angles θ from the chain. The projection of the wave number of the incident electromagnetic wave to the chain is zero in the present geometry. The lowest peak decreases more rapidly than $\cos^2(\pi/2-\theta)$, which is expected from the dipole radiation pattern. This means that the system becomes momentum selective when the size becomes comparable with the wavelength.

We have also calculated the response spectra by discarding all matrix elements, except the diagonal elements of A. It has been found that the difference is negligibly small for the range of the energy and the size shown here. As N becomes larger, A tends to be diagonal because of the conservation of the momentum and the orthogonality of the transition dipole moments. These facts suggest that the radiative (real) shift and radiative width are dominated by the diagonal elements of A.

Figure 4 shows the N dependence of the radiative width and (real) shift for the modes with the transition dipole moments parallel and perpendicular to the chain. They are estimated from both of the response spectra and the diagonal elements of A. Only the modes whose radiative width is larger than that of a single sphere are shown. This criterion is also used in the following fig-

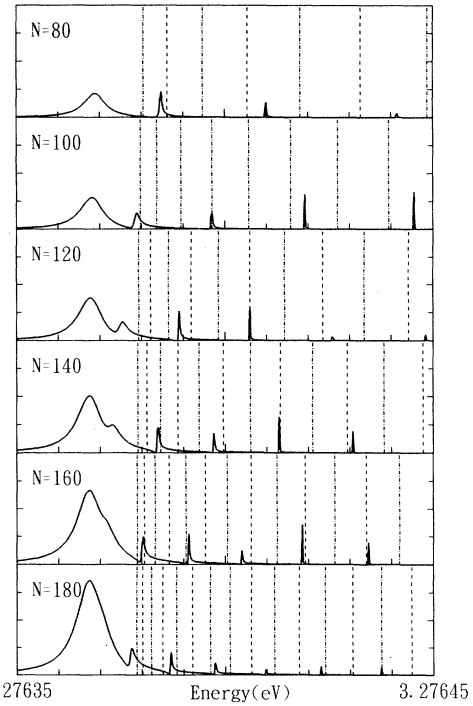

FIG. 2. The response spectra of the chains with $N = 80 \sim 180$. The geometry is the same as in Fig. 1.

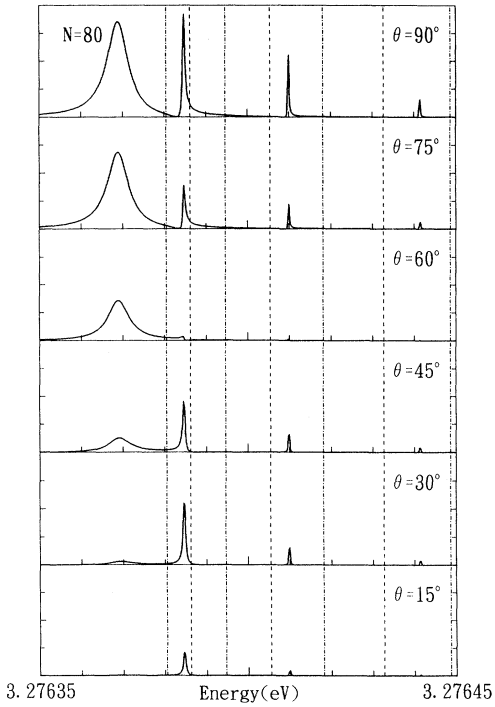

FIG. 3. The response spectra for the chain with $N = 80$ observed in the direction at various angles θ from the chain. The other condition of the geometry is the same as in Fig. 1.

ures. The filled and open circles correspond to the modes with even and odd parities, respectively. The horizontal dash-dotted lines depict the values of the modes with $\mathbf{k} = \mathbf{0}$ in the infinite chain. The radiative width grows monotonously to the limiting value in (a), while it once overshoots in (c). The imaginary part of A in the infinite chain, has a maximum at $k_\lambda = 0$ and a minimum at $k_\lambda = q$ for the polarization parallel to the chain, while the relation is opposite for the polarization perpendicular to the chain, as seen in Eq. (4.20). This fact and the consideration of the averaging mentioned in the last section explains the difference in the limiting behavior of the radiative width.

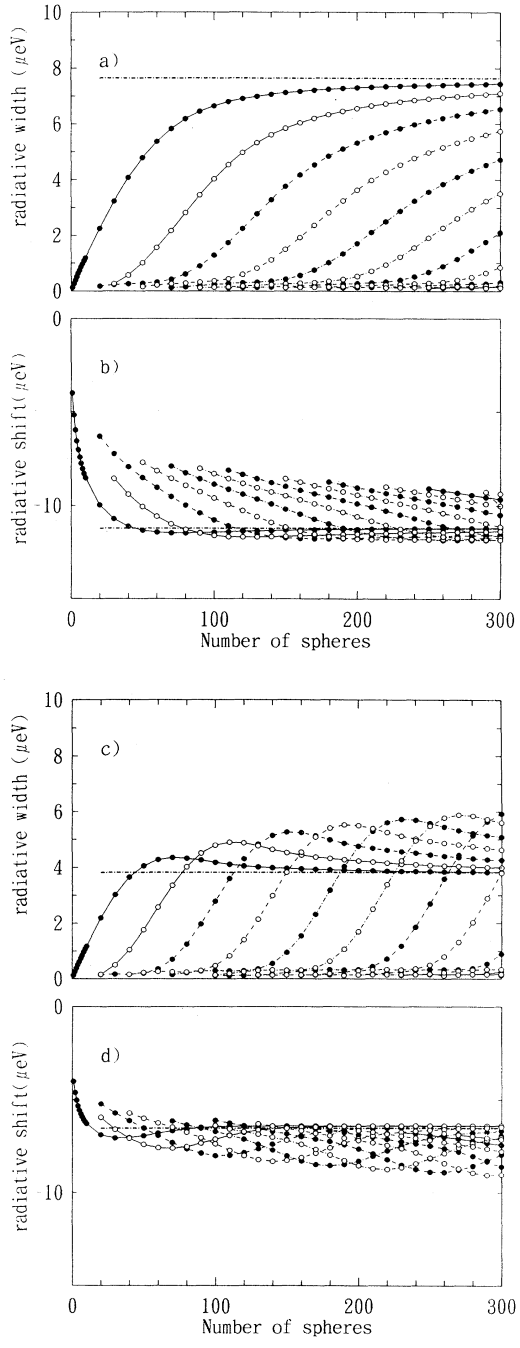

FIG. 4. The dependence on the number of the spheres of the radiative width and the radiative shift in the linear chain. The polarization is parallel to the chain in (a) and (b), and perpendicular to it in (c) and (d). The filled and open circles correspond to the modes with even and odd parities, respectively. The horizontal dash-dotted lines depict the values of the modes with $\mathbf{k} = \mathbf{0}$ in the infinite chain.

B. $D = 2$

Figure 5 shows the radiative width and shift for the modes, whose transition dipole moments are perpendicular to the plane of the square system. The filled and open squares correspond to the modes with and without a net dipole moment, respectively. Because the linear dimension of the system is still smaller than the wavelength of the resonant light even for the largest size, the saturation is not as clear as in the linear chain. The behavior is, however, almost similar. It should be noted that only the states with a net dipole moment interact with radiation fields in the LWA theory. This criterion approximately works only when the system is much smaller than the wavelength of light in the present theory. The figure shows that the LWA is not valid when the linear dimension is larger than $20b \sim 1000$ Å.

In Fig. 6, the N dependence of the radiative width and shift are shown for the states with the transition

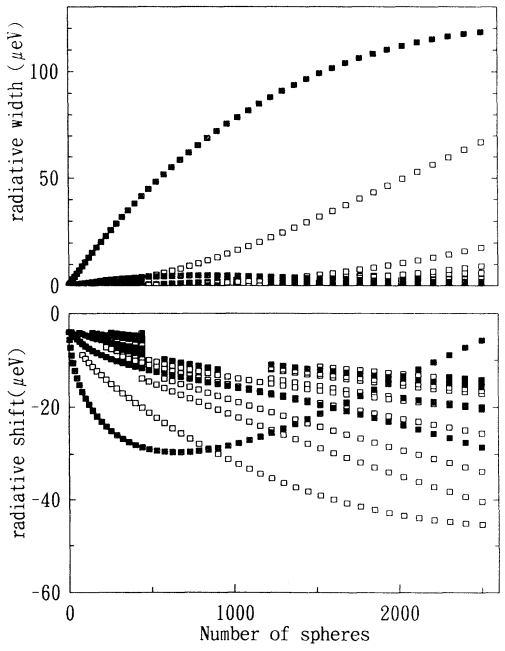

FIG. 5. The dependence on the number of the spheres of the radiative width and the radiative shift in the square system. The transition dipole moments are perpendicular to the plane. The filled and open squares correspond to the modes with and without a net dipole moment, respectively.

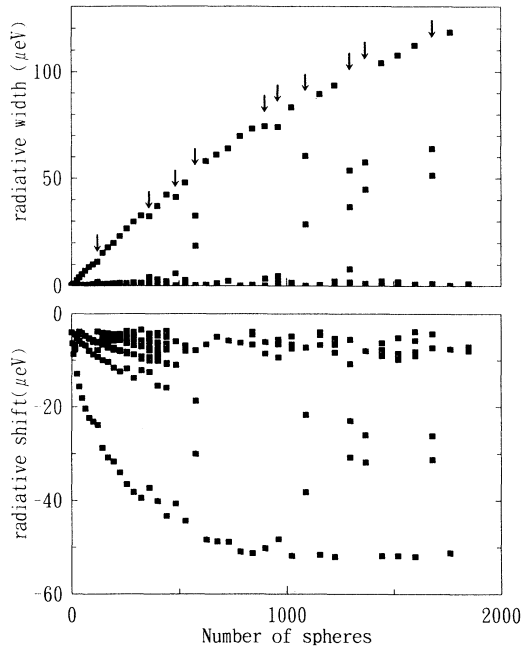

FIG. 6. The dependence on the number of the spheres of the radiative width and shift in the square system. Transition dipole moments lie in the plane.

dipole moments lying in the plane. For simplicity, only the width and shift of the states with a net dipole moment are shown. Unlike Fig. 5, there are some dips at the points indicated by arrows if we follow the mode with the largest radiative width. Other modes with considerably large radiative width appear there. The radiative width is divided according to the sum rule mentioned earlier. It should be noted that the number of degrees of freedom, N_L, is two in the present case. The states with a net dipole moment, however, appear in pairs of linearly independent states, because of C_4 symmetry. This is why the sum of the shown radiative corrections is almost the same as in Fig. 5. The small difference is attributed to the states without a net dipole moment.

In order to see what happens when the dips appear, the dipole moments of the corresponding states are shown for $N = 3^2$, 4^2, and 5^2 in Fig. 7. When $N = 4^2$, for which the first dip appears, there are two states which have similarly large net dipole moments and close excitation energies. Once such states appear, they have to share the total available radiative width and thereby the width of each must be small. If the dipole-dipole interaction is truncated within the nearest neighbors, the eigenstates can be described as a direct product of the states in the linear system. Then the dips would disappear. The dips are attributed to the long-range nature of the dipole-dipole interaction.

C. $D = 3$

The partition of the radiative width seen in the two-dimensional system is more significant in the three-dimensional systems. Figure 8 shows the N dependence of the radiative width and shift in the cubic system. More modes appear with comparable radiative widths even for small N and no size-linear dependence is visible for $N > 3^3$. It should be noted that the linear dimension of the largest system considered here is about 350 Å,

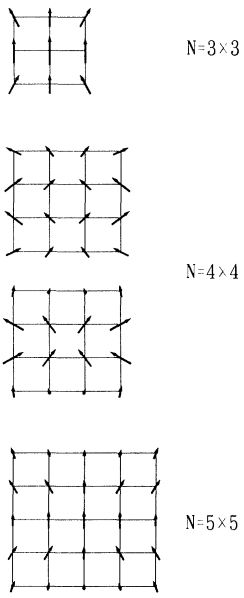

FIG. 7. The dipole moments of the states which have a large total dipole moment in the square systems with $N = 3^2$, 4^2, and 5^2.

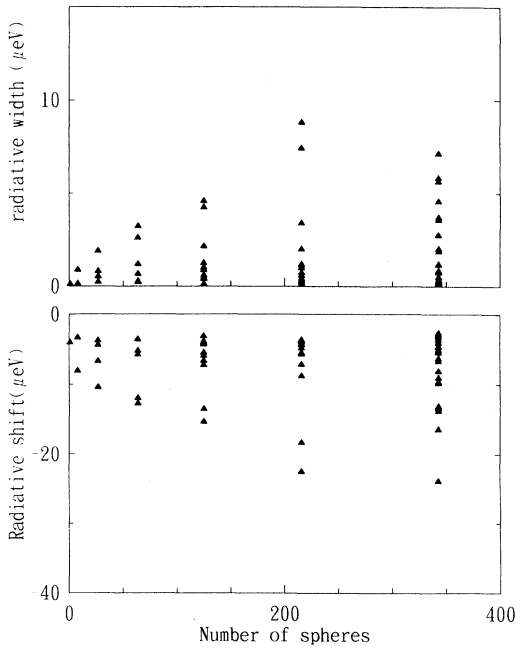

FIG. 8. The dependence on the number of the spheres of the radiative width and shift in the cubic system.

which is 1/10 as small as the wavelength of the resonant light.

D. Nonlocality induced double resonance in energy and size condition in linear systems

The resonant energies $\tilde{E}_\lambda$'s are shifted from the excitation energies E_λ's of the unperturbed systems, due to the radiative correction as investigated so far. Here, we consider the NIDORES condition, which has been introduced in Sec. I. Figure 2 shows how E_λ's and $\tilde{E}_\lambda$'s move, as the length of the array of the fine particles is changed. (Because of the geometry, only the peaks corresponding to the states with even parity are visible in the response spectra.) As the system becomes longer, the size-quantization effect becomes smaller and the energy separation between E_λ's gets narrower. The radiative shift becomes larger on the other hand. We will label the state according to the ascending order of the nodes of the wave functions. (For the states with dipole moment parallel to the chain, the lowest state corresponds to $\lambda = 1$, while the highest does to $\lambda = 1$ for the states with dipole moment perpendicular to the chain.) When $N \sim 100$, the second lowest peak (corresponding to $\tilde{E}_3$) crosses the position of the lowest excitation energy E_1 in Fig. 2. The dipole pattern corresponding to the E_3 state is resonantly induced if the energy of the incident light is fixed to E_1. The peak goes to the lower energy side for larger N, but a similar situation occurs again for $N \sim 180$, where the third lowest peak (corresponding to $\tilde{E}_5$) passes E_1. Figure 9 shows the size dependence of $|F_\lambda|^2$, where F_λ's are the expansion coefficients of the polarization $\mathbf{P}$ [see Eq. (2.8)]. The energy of the incident light is fixed to E_1. The periodic resonant enhancement of the polarization is clearly shown.

Such resonant enhancement is generally expected.[14] The behavior is, however, considered to have a variety according to the energy dispersion, the energy separation, the radiative shift and width, the coupling to the incident field, and their dependence on the size and the geometry, etc. In Fig. 10, the size dependence of $|F_\lambda|^2$ is shown for the polarization perpendicular to the chain.

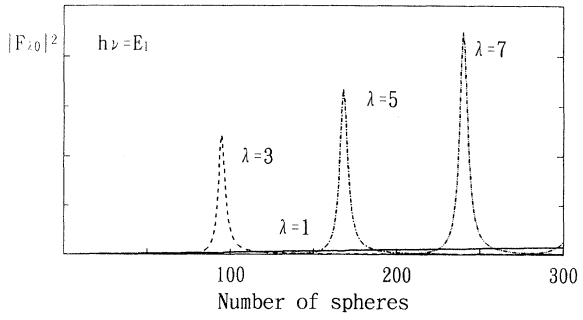

FIG. 9. The size dependence of $|F_\lambda|^2$'s for the polarization parallel to the chain. The incident light comes perpendicularly to the chain. The energy of the incident light is fixed to E_1.

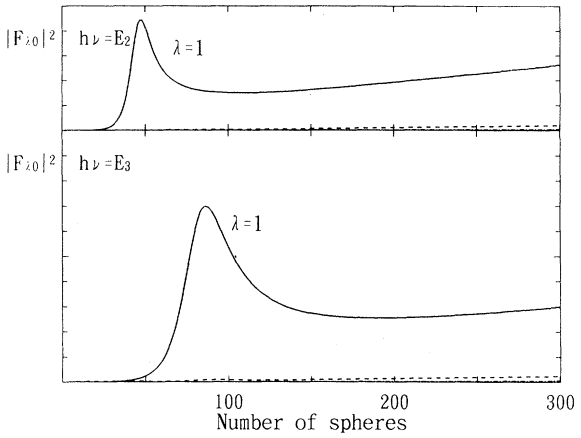

FIG. 10. The size dependence of $|F_\lambda|^2$ for the polarization perpendicular to the chain. The incident light comes perpendicularly to the chain. The energy of incident light is fixed to E_2 and E_3 in (a) and (b), respectively.

The incident light comes perpendicularly to the chain. The energy of incident light is fixed to E_2 and E_3 in (a) and (b), respectively. The $|F_1|^2$ has a peak, but also has a large tail linearly increasing with the size in this case. The difference results from the following facts. The radiative correction and the coupling to the incident field, $c_\lambda^{(0)}$, determine F_λ. The radiative correction to E_1 is already saturated for $N \sim 50$ in case of the present geometry, while those to E_λ ($\lambda = 3, 5, 7$) are not. The linear growth shown in Fig. 10 comes from the linear growth of $|c_1^{(0)}|^2$. If the dipole interaction is truncated within the nearest neighbors, the dipole density has a form as

$$\boldsymbol{\rho}_\lambda = \sum_m \boldsymbol{\rho}^0_{m\xi} \sqrt{\frac{2}{N}} \sin \frac{\pi \lambda m}{N+1} . \tag{5.1}$$

This is found numerically to be a good approximation in the one-dimensional case. Using the above expression, we have

$$c_\lambda^{(0)} = \boldsymbol{\mu}_\xi \cdot \mathbf{E}_0 \sqrt{\frac{2}{N}} \cot \frac{\pi \lambda}{N+1} , \tag{5.2}$$

where $\mathbf{E}_0$ is the coefficient vector of the incident electric field. The $c_\lambda^{(0)}$ is proportional to $\sqrt{N}$ if N is large. Figure 11 shows the size dependence of $|F_\lambda|^2$ for the incident light coming in parallel to the chain with the polarization perpendicular to it. The energy of incident light is also fixed to E_2 and E_3 in (a) and (b), respectively. It should be noted that only the propagating direction of the incident field is different in the geometries used for Figs. 10 and 11. The projection of the wave number of the incident light is finite in Fig. 11, while it is zero in Fig. 10. Only the states with the same wave number component as the projection of the wave number of the incident light can be excited. In a small system, the distribution of the wave number is broad. As the system becomes long, the states have a sharper distribution of the wave number.

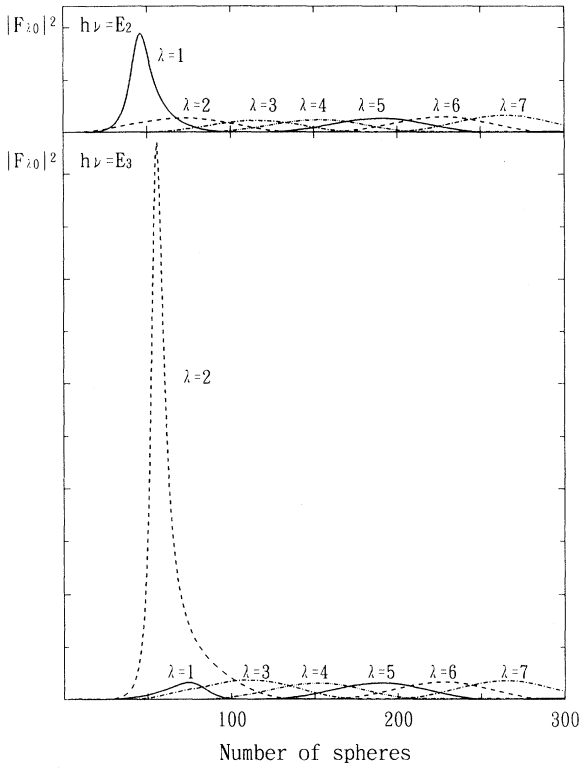

FIG. 11. The size dependence of $|F_\lambda|^2$ for the incident light coming in parallel to the chain with the polarization perpendicular to it. The energy of incident light is also fixed to E_2 and E_3 in (a) and (b), respectively.

The state with $\lambda = 1$ is always strongly excited if the incident light propagates perpendicular to the chain, while the coupling of the state with the incident light propagating along the chain becomes weaker as the system becomes larger. This yields the difference between Figs. 10 and 11.

VI. DISCUSSION

We have studied with a great interest in the complex radiative correction how the size and the geometry of matter systems affect their optical responses, applying a nonlocal theory to a model of assemblies of semiconductor spheres. The obtained results take advantage of the theory, which is free from the boundary condition. The change of the radiative correction with increasing the system size has been investigated numerically for different geometries. In particular, the change from one sphere to an infinite chain of the spheres has been demonstrated. It has been shown that the radiative correction is significantly affected by the geometry as well as the size, even if the system is much smaller than the wavelength of the resonant light. The radiative width deviates from the linear dependence on the size at a smaller size in a higher dimension. As mentioned in Sec. I, the volume-linear dependence has been confirmed experimentally for CuCl microcrystallites, but deviation has been observed when the radii is larger than 5 nm.[8] The critical radius seems smaller than the one at which the long wavelength approximation loses validity. One of the reasons may be the effect of the other neglected degrees of freedom such as phonons, for temperature dependence has also been observed.[8] The critical radius is, however, too small even at $T = 10$ K. Although we cannot directly compare the present results with the experiment, the experiment may reflect the three-dimensional nature of the microcrystallites. The NIDORES condition has also been investigated for chains of the spheres. The effect is common, but shows a variety of behaviors specific to geometrical factors. This effect is expected to lead to a more precise description of the radiation-matter interaction.

ACKNOWLEDGMENTS

This work is supported in part by the Grant-in-Aid for Scientific Research from Ministry of Education, Science and Culture of Japan. The numerical calculation was carried out on SX-3 in the computation center of Osaka University. The authors are grateful to Professor K. Makoshi for critical comments. Fruitful discussions with Professor J. Pendry is also acknowledged.

APPENDIX A: POSITION OF THE NONLOCAL FORMALISM AMONG THE KNOWN FRAMEWORKS OF RESPONSE THEORIES

In order to clarify the positioning of the nonlocal response theory among the known frameworks of response theories, we add this appendix. In any optical response theory, we need to determine the electromagnetic (EM) field produced as a result of the interaction of an incident EM field and a given material system. Since the motions of EM field and matter interact with each other, we have to fix the motions self-consistently. In order to achieve this in a semiclassical framework, we need the following steps.

For a clear definition of matter and EM field, we take Coulomb gauge ($\mathrm{div}\mathbf{A} = 0$). In this gauge, the scalar potential $\phi(\mathbf{r}, t)$ is the full instantaneous Coulomb interaction of all the charged particles in the system, and we regarded it as a part of matter Hamiltonian H_0. Then, the EM field is purely transverse, represented by $\mathbf{A}(\mathbf{r}, t)$, and the radiation-matter interaction H_{int} is the sum of

$$-\frac{e}{mc}\mathbf{p}\cdot\mathbf{A} + \frac{e^2}{2mc^2}\mathbf{A}^2 , \tag{A1}$$

for all the charged particles.

The quantities to be determined self-consistently are $\mathbf{A}$ and current density $\mathbf{j}(\mathbf{r}, t)$. [Of course, one may translate them into electric field $\mathbf{E}_s(\mathbf{r}, t)$ and induced polarization $\mathbf{P}(\mathbf{r}, t)$.] The motion of charged particles (EM field) is determined by Schrödinger (microscopic Maxwell) equation(s). Thus, we obtain $\mathbf{A}$ as a functional of $\mathbf{j}$ from

microscopic Maxwell equations, which have $\mathbf{j}$ and ϕ as source terms, as

$$\mathbf{A}(\mathbf{r},t)=\mathbf{A}_0(\mathbf{r},t)+\mathcal{G}[\mathbf{j}]\ , \tag{A2}$$

where $\mathbf{A}_0$ is the free (incident) field. Since $\mathbf{j}$ and ϕ are related via continuity equation, $\mathcal{G}$ is a functional of $\mathbf{j}$ alone. From the Schrödinger equations for the Hamiltonian $H_0+H_{\rm int}$, we can determine the time development of matter wave function, from which we can calculate the expectation values of any physical quantities as c numbers. The current density $\mathbf{j}$ is determined in such a way as a functional of $\mathbf{A}$:

$$\mathbf{j}(\mathbf{r},t)=\mathcal{F}[\mathbf{A}]\ , \tag{A3}$$

where we assume that $\mathbf{j}=0$ in the absence of $\mathbf{A}$, as usual. From these two equations (A2) and (A3), we can determine $\mathbf{A}$ and $\mathbf{j}$ self-consistently for a given initial condition (of matter and radiation field). The forms of the functionals are as follows. The ω-Fourier component of $\mathcal{G}$ is

$$\begin{aligned}\hat{\mathcal{G}}(\mathbf{r},\omega)=&\int g_q(\mathbf{r}-\mathbf{r}')\mathbf{j}(\mathbf{r}',\omega)d\mathbf{r}'\\&+\frac{1}{q^2}\int[g_q(\mathbf{r}-\mathbf{r}')\\&-g_0(\mathbf{r}-\mathbf{r}')]\ \text{grad div}\ \mathbf{j}(\mathbf{r}',\omega)d\mathbf{r}'\ ,\end{aligned} \tag{A4}$$

$$g_q(\mathbf{r})=\frac{e^{iq|\mathbf{r}|}}{|\mathbf{r}|}\qquad(q=\omega/c)\ . \tag{A5}$$

The functional $\mathcal{F}$ contains $\mathbf{A}$ up to the infinite order, in general, as

$$\begin{aligned}\hat{\mathcal{F}}(\mathbf{r},\omega)=&\int\chi^{(1)}(\mathbf{r},\mathbf{r}',\omega)\mathbf{A}(\mathbf{r}'\omega)d\mathbf{r}'\\&+\sum_{\omega_1}\sum_{\omega_2}\int\int\chi^{(2)}(\mathbf{r},\mathbf{r}_1,\mathbf{r}_2,\omega_1,\omega_2)\\&\times\mathbf{A}(\mathbf{r}_1,\omega_1)\mathbf{A}(\mathbf{r}_1,\omega_2)d\mathbf{r}_1d\mathbf{r}_2\\&+\cdots\ ,\end{aligned} \tag{A6}$$

where the integral kernels are called linear, second- (third-, ...) order nonlinear "susceptibilities."

The branching point for various response theories lies in the treatment of the susceptibilities $\chi^{(j)}$. According to the quantum mechanical perturbation treatment, they are functions of various coordinates. In the nonlocal theory, we keep its position dependence as required by quantum mechanics, while, in the traditional response theory, one makes local approximation to them as, for example,

$$\chi^{(1)}(\mathbf{r},\mathbf{r}',\omega)\cong\bar{\chi}^{(1)}(\omega)\delta(\mathbf{r}-\mathbf{r}')\ . \tag{A7}$$

If one considers EM fields as a macroscopically averaged field, this assumption often holds rather well. This local approximation means that the induced current (or polarization) at point $\mathbf{r}$ depends only on the fields at the same point. If the point $\mathbf{r}$ describes a "macroscopically small but microscopically large volume," as in the traditional response theory, it may well be a reasonable approximation. However, in (microscopic and) mesoscopic systems, we need a microscopic description of EM field, and we must keep the nonlocality as required by quantum mechanics. In this way, it is clear that the nonlocal theory is closer to the first principles than the local one.

The feasibility of solving (A2) and (A3) in nonlocal manner is supported very much by the separable nature of the integral kernels, which is valid for resonant processes, in general. In such a case, the equations are reduced to a set of simultaneous Nth order polynomial equations, where, N is the order of the nonlinearity in consideration. In this paper, the case $N=1$ is treated.

In Ref. 10, the relation (A2) is described as the one among the source ($\mathbf{E}_s$), Maxwell ($\mathbf{E}_M$), and depolarization ($\mathbf{E}_{\rm dep}$) fields as

$$\mathbf{E}_s=\mathbf{E}_M-\mathbf{E}_{\rm dep}\ . \tag{A8}$$

If one notes $\mathbf{E}_s=iq\mathbf{A}$ and $\mathbf{j}(\mathbf{r},\omega)=-i\omega\mathbf{P}(\mathbf{r},\omega)$, (A2) is certainly rewritten as Eq. (A8), where

$$\mathbf{E}_M=\tilde{\mathbf{E}}+\frac{1}{q^2}\text{grad div}\ \tilde{\mathbf{E}}\ ,$$

$$\tilde{\mathbf{E}}(\mathbf{r},\omega)=q^2\int g_q(\mathbf{r}-\mathbf{r}')\mathbf{P}(\mathbf{r}')d\mathbf{r}'\ ,$$

$$\tilde{\mathbf{E}}_{\rm dep}(\mathbf{r},\omega)=q^2\int g_0(\mathbf{r}-\mathbf{r}')\text{grad div}\ \mathbf{P}(\mathbf{r}')d\mathbf{r}'\ ,$$

$$(\text{rot rot}\ -q^2)\mathbf{E}_M=4\pi q^2\mathbf{P}\ .$$

In this way, we can reconfirm that the basic relation Eq. (A8) used in Ref. 10 is the solution of microscopic Maxwell equations.

The nonrelativistic QED starts with the same Hamiltonian $H_0+H_{\rm int}$ added with free-field Hamiltonian H_F, and then quantizes $\mathbf{A}$ included in $H_{\rm int}$ and H_F. One can show that the Eqs. (A2) and (A3) are the c-number versions of the QED equations of motions for the operators $\mathbf{A}$ and $\mathbf{j}$. (There is precise coincidence of the coefficients between the set of equations.) The nonlocal theory should be placed just below the nonrelativistic QED, and above the local response theory as a semiclassical scheme.

APPENDIX B: CALCULATION OF $A^{(1)}$

We calculate $A^{(1)}_{\lambda\mu}$ for an infinite linear chain. Putting Eqs. (4.2), (4.3), and (4.12) into Eq. (4.1) yields

$$\begin{aligned}A^{(1)}_{\lambda\mu}=\delta_{\mathbf{k}_\lambda,\mathbf{k}_\mu}\Bigg\{&\hat{A}^{(0)}_{\lambda\mu}+V_s^2(qR)\sum_{\ell=1}^{3}I^{(\ell)}\\&\times\Big\{E_\ell[(q+k_\lambda)b]+E_\ell[(q-k_\lambda)b]\Big\}\\&-I^{(3)}[E_3(k_\lambda b)+E_3(-k_\lambda b)]\Bigg\},\end{aligned} \tag{B1}$$

where

$$I^{(1)} = \frac{q^2}{b}[\hat{\boldsymbol{\mu}}_\lambda \cdot \hat{\boldsymbol{\mu}}^*_\mu - (\hat{\mathbf{k}}_\lambda \cdot \hat{\boldsymbol{\mu}}_\lambda)(\hat{\mathbf{k}}_\mu \cdot \hat{\boldsymbol{\mu}}^*_\mu)] , \tag{B2}$$

$$I^{(2)} = i\frac{q}{b^2}[\hat{\boldsymbol{\mu}}_\lambda \cdot \hat{\boldsymbol{\mu}}^*_\mu - 3(\hat{\mathbf{k}}_\lambda \cdot \hat{\boldsymbol{\mu}}_\lambda)(\hat{\mathbf{k}}_\mu \cdot \hat{\boldsymbol{\mu}}^*_\mu)] , \tag{B3}$$

$$(= -iqbI^{(3)}) ,$$

$$I^{(3)} = -\frac{1}{b^3}[\hat{\boldsymbol{\mu}}_\lambda \cdot \hat{\boldsymbol{\mu}}^*_\mu - 3(\hat{\mathbf{k}}_\lambda \cdot \hat{\boldsymbol{\mu}}_\lambda)(\hat{\mathbf{k}}_\mu \cdot \hat{\boldsymbol{\mu}}^*_\mu)] , \tag{B4}$$

and

$$E_\ell(x) \equiv \sum_{n=1}^{\infty} \frac{e^{ixn}}{n^\ell} . \tag{B5}$$

We have replaced $\hat{\mathbf{r}}_{mn}$'s by $\hat{\mathbf{k}}_\lambda$'s because all of them are the identical unit vector parallel to the chain. (Though the orientation may be different, they always appear in pair.) The $\hat{A}^{(0)}_{\lambda\mu}$ is obtained from $A^{(0)}_{\lambda\mu}$ by replacing $\boldsymbol{\mu}_\xi$ and $\boldsymbol{\mu}^*_\eta$ by $\hat{\boldsymbol{\mu}}_\lambda$ and $\hat{\boldsymbol{\mu}}^*_\mu$, respectively. The E_ℓ's satisfy

$$E_\ell(x + 2\pi) = E_\ell(x) , \tag{B6}$$

$$E_{\ell-1}(x) = -i\frac{d}{dx}E_\ell(x) . \tag{B7}$$

The $E_0(x)$ can be easily evaluated for $\mathrm{Im}x \downarrow 0$. The other E_ℓ's are obtained by integration according to Eq. (B7) with the use of $E_1(\pi) = -\ln 2$ and $E_\ell(0) = \zeta(\ell)$ for $\ell \geq 2$. The E_ℓ's are given for $0 \leq x \leq 2\pi$ by

$$E_1(x) = -\ln\left(2\sin\frac{x}{2}\right) - \frac{i}{2}(x - \pi) , \tag{B8}$$

$$E_2(x) = \frac{1}{4}(x - \pi)^2 - \frac{\pi^2}{12} - i\left(x\ln 2 + \int_0^x dt \ln\sin\frac{t}{2}\right) , \tag{B9}$$

$$E_3(x) = \zeta(3) + \frac{1}{2}x^2\ln 2 + \int_0^x dt(x - t)\ln\sin\frac{t}{2} + \frac{i}{12}x(x - \pi)(x - 2\pi) . \tag{B10}$$

The definition range is extended according to Eq. (B6), which leads

$$E_\ell(x) = \sum_n \theta(x - 2\pi n)\theta[2\pi(n + 1) - x]E_\ell(x - 2\pi n) , \tag{B11}$$

where the Heaviside function appears to ensure that the argument of E_ℓ on the right hand side is in the above definition range. Putting the explicit forms of E_ℓ's into Eq. (B1), we have

$$A^{(1)}_{\lambda\mu} = \delta_{\mathbf{k}_\lambda,\mathbf{k}_\mu}\left\{\hat{A}^{(0)}_{\lambda\mu} + V_s^2(qR)\sum_{\ell=1}^{3} I^{(\ell)} f_\ell(q, k_\lambda) - I^{(3)} f_3(0, k_\lambda)\right\} , \tag{B12}$$

where

$$f_1(q, k_\lambda) = \sum_n \theta(q_n + k_\lambda)\theta(2\pi - q_n - k_\lambda) \times\left\{ - \ln 2|\cos k_\lambda b - \cos q_n b| - iq_n b + i\pi\theta(q_n - k_\mu)\right\}_{q_n = q - \frac{2\pi n}{b}} , \tag{B13}$$

$$f_2(q, k_\lambda) = \sum_n \theta(q_n + k_\lambda)\theta(2\pi - q_n - k_\lambda) \times\left\{ - i\left(2q_n b\ln 2 + \int_0^{(q_n + k_\lambda)b} \ln\sin\frac{t}{2}dt + \int_0^{(q_n - k_\lambda)b} \ln\left|\sin\frac{t}{2}\right|dt\right) + \frac{b^2}{2}(q_n^2 + k_\lambda^2) - \pi k_\lambda b + \frac{\pi^2}{3} - \pi(q_n - k_\lambda)b\theta(q_n - k_\lambda)\right\}_{q_n = q - \frac{2\pi n}{b}} , \tag{B14}$$

$$f_3(q, k_\lambda) = \sum_n \theta(q_n + k_\lambda)\theta(2\pi - q_n - k_\lambda)\left\{2\zeta(3) + (q_n^2 b^2 + k_\lambda^2 b^2)\ln 2 + \int_0^{(q_n + k_\lambda)b} [(q_n + k_\lambda)b - t]\ln\sin\frac{t}{2}dt + \int_0^{(q_n - k_\lambda)b} [(q_n - k_\lambda)b - t]\ln\left|\sin\frac{t}{2}\right|dt + i\left(\frac{1}{6}q_n^3 b^3 + \frac{1}{2}q_n k_\lambda^2 b^3 - \pi q_n k_\lambda b^2 + \frac{\pi^2}{3}q_n b - \frac{\pi}{2}(q_n - k_\lambda)^2 b^2\theta(q_n - k_\lambda)\right)\right\}_{q_n = q - \frac{2\pi n}{b}} , \tag{B15}$$

$$f_3(0, k_\lambda) = 2\zeta(3) + k_\lambda^2 b^2\ln 2 + 2\int_0^{k_\lambda b} [k_\lambda b - t]\ln\sin\frac{t}{2}dt . \tag{B16}$$

[1] N. Ochi, T. Shiotani, M. Yamanishi, Y. Honda, and I. Suemune, Appl. Phys. Lett. **58**, 2735 (1991).
[2] E. Hanamura, Phys. Rev. B **38**, 1228 (1988).
[3] K. Cho, M. Nishida, Y. Ohfuti, and L. Belleguie, J. Lumin. **60&61**, 330 (1994).
[4] Y. Ohfuti and K. Cho, *Science and Technology of Mesoscopic Structures*, edited by S. Nambda, C. Hamaguchi, and T. Ando (Springer Verlag, 1992), p. 457.
[5] Y. Ohfuti and K. Cho, Jpn. J. Appl. Phys. **9**, 197 (1993).
[6] E. Hanamura, Phys. Rev. B **37**, 1273 (1988).
[7] H. Ishihara and K. Cho, J. Nonlinear Opt. Phys. **1**, 287 (1992).
[8] T. Itoh, M. Furumiya, T. Ikehara, and C. Gourdon, Solid State Commun. **73**, 271 (1990).
[9] M. Orrit, C. Aslangul, and P. Kottis, Phys. Rev. B **25**, 7263 (1982).
[10] K. Cho, Prog. Theor. Phys. Suppl. **106**, 225 (1991).
[11] P. W. Milonni, J. R. Ackerhalt, and W. A. Smith, Phys. Rev. Lett. **31**, 958 (1973).
[12] J. Dalibard, J. Dupont-Roc, and C. Cohen-Tannudji, J. Phys. (Paris) **43**, 1617 (1982).
[13] H. Ishihara and K. Cho, in *Science and Technology of Mesoscopic Structures* (Ref. 4), p. 464.
[14] K. Cho, H. Ishihara, and Y. Ohfuti, Solid State Commun. **87**, 507 (1993).
[15] The functional form of $\boldsymbol{\rho}^0_{m\xi}(\mathbf{r})$ is slightly different from that in Refs. 4 and 5, where a uniform transition dipole density is assumed. But the results are qualitatively similar.
[16] Since the system Hamiltonian contains the whole Coulomb interaction, $E_{\rm dep}$ is better called the self-interaction energy of induced polarization.
[17] C. F. Bohren and D. Huffman, *Absorption and Scattering of Light by Small Particles* (Wiley, New York, 1983), Appendix A.
[18] In their book, 1 in the expression $x + 4x^{1/3} + 1$ is replaced by 2, because they were discussed in terms of N and M fields.
[19] The corresponding expression in Ref. 5 is valid when $\hat{\boldsymbol{\mu}}_\lambda$'s lie in the plane.